

VARIABLE-ORDER FRACTIONAL CREEP MODEL OF MUDSTONE UNDER HIGH-TEMPERATURE

by

Ming LI^a, Hai PU^{a,b*}, and Lili CAO^a

^a State Key Laboratory for Geomechanics and Deep Underground Engineering,
China University of Mining and Technology, Xuzhou, China

^b School of Mechanics and Civil Engineering, China University of Mining and Technology,
Xuzhou, China

Original scientific paper
<https://doi.org/10.2298/TSCI17S1343L>

In order to study the properties of high-temperature creep for mudstone, MTS810 electro-hydraulic servo material test system and MTS652.02 high temperature furnace are utilized for the creep test of mudstone at 700 °C. Considering the visco-elastic-plastic characteristics and the damage effect, the variable-order fractional creep model is established to research the creep character; and it is found that the proposed model can be well fitting of our experimental results. Especially, variable-order function can be used to analyze and study the viscoelastic property evolution of mudstone in process of high-temperature creep. Compositions of mudstone are distinguished by X-ray diffraction technology. The presence of the illite under high temperatures can be used for explaining the viscous feature prevails over the elastic ones in viscoelastic properties.

Key words: *high temperature, variable-order, creep model, mudstone*

Introduction

Creep is one of the most important causes of surrounding rock deformation and instability. For engineering works involving coal-bed gas exploitation, development of geothermal resources, and underground storage of highly radioactive nuclear waste, the deformation behaviors of surrounding rock are also affected by temperature. Concerning the influence of both temperature and pressure, long-term deformation of surrounding rock have been considered the key factors affecting the safe and efficient mining of resources, space security, and stability for nuclear waste disposal. Thus, creep behaviors under high temperature are crucial for the development of the above engineering projects.

With the development of fractional calculus, the researches on fractional calculus have drawn lots of attentions from various fields [1-3]. Especially, fractional order viscoelastic material models also widely studied [4-7]. Variable-order fractional calculus, the generalization of fractional calculus theory, is presented as a useful tool nowadays, with successful applications in mechanics [8], in the modelling of linear and nonlinear viscoelasticity oscillators [9, 10] and in other phenomena where the order of the derivative varies with time [11, 12]. The effect of differences between using constant and variable-order fractional derivatives has been

* Corresponding author, e-mail: puhaicumt@163.com

discussed [13]. Differential equations which consist of variable-order became a field of interest for many researches including the analytic results [14-16] and the numerical analysis [17-22].

However, the rock compositions may change with the influence of temperature and chemical erosion in reality, leading to the variation of viscoelastic properties. Therefore, we gave the variable-order fractional creep model to study the creep characteristics and viscoelastic evolution of mudstone at 700 °C. Testing the mudstone composition at 700 °C was used to specify the revolution of viscoelastic properties.

Variable order damaging creep model

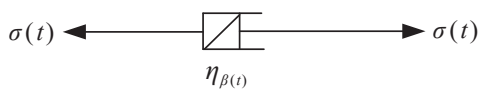


Figure 1. Variable order Abel dashpot
When the stress $\sigma(t) = \sigma_0$, the strain $\varepsilon(t) = \eta_{\beta(t)} \left({}_0 D_t^{\beta(t)} \varepsilon \right)(t)$.
Therefore, the variable-order fractional Abel dashpot, fig 1, can be expressed as:

$$\sigma(t) = \eta_{\beta(t)} \left({}_0 D_t^{\beta(t)} \varepsilon \right)(t) \quad 0 \leq \beta(t) \leq 1 \quad (1)$$

There are some differences in viscoelastic properties of the same rock materials under different conditions. Thus, in order to accurately describe the viscoelastic characteristics of rock materials in the creep process under different conditions, the variable-order fractional Abel dashpot, fig 1, can be expressed as:

$$\varepsilon(t) = \left({}_0 D_t^{-\beta(t)} \frac{\sigma_0}{\eta_{\beta(t)}} \right) \quad (2)$$

Without loss of generality, when $\beta(t)$ is piecewise function: *i. e.*

$$\beta(t) = \beta_n, \quad t \in (t_{n-1}, t_n] \quad (n = 1, 2, \dots, N)$$

The strain (ε) can be calculated in detail as follows: when $t \in (t_{n-1}, t_n]$, we can get to the result:

$$\begin{aligned} \varepsilon_{ve}(t) &= \frac{1}{\eta_{\beta_1}} \int_0^{t_1} \frac{(t-\tau)^{\beta_1-1}}{\Gamma(\beta_1)} \sigma_0 d\tau + \frac{1}{\eta_{\beta_2}} \int_{t_1}^{t_2} \frac{(t-\tau)^{\beta_2-1}}{\Gamma(\beta_2)} \sigma_0 d\tau + \dots + \frac{1}{\eta_{\beta_n}} \int_{t_{n-1}}^t \frac{(t-\tau)^{\beta_n-1}}{\Gamma(\beta_n)} \sigma_0 d\tau = \\ &= \sum_{i=1}^{n-1} \frac{1}{\eta_{\beta_i}} \frac{(t_i - t_{i-1})^{\beta_i}}{\Gamma(\beta_i + 1)} \sigma_0 + \frac{\sigma_0}{\eta_{\beta_n} \Gamma(\beta_n + 1)} (t - t_{n-1})^{\beta_n} \end{aligned} \quad (3)$$

Since the accelerating creep occurs only if the stress level exceeds the yield stress, a damaged fractional order Abel element is used to characterize the viscoplastic body. Consequently, the constitutive relation is described as:

$$\sigma_{vp} - \sigma_s = \eta_s e^{-\lambda t} \frac{d^\gamma \varepsilon_{vp}(t)}{dt^\gamma} \quad (4)$$

When $\sigma(t) = \sigma_0$, the creep can be expresses as:

$$\varepsilon_{vp}(t) = \frac{\sigma_0 - \sigma_s}{\eta_s} t^\gamma E_{1,1+\gamma}(\lambda t) \quad (5)$$

where

$$E_{1,1+\gamma}(\lambda t) = \sum_{k=0}^{\infty} \frac{(\lambda t)^k}{\Gamma(k+1+\gamma)}$$

Finally, we propose the variable order damaged creep model, fig. 2, and the creep relation can be expressed based on the eq. (3) and eq. (5):

$$\varepsilon(t) = \begin{cases} \sum_{i=1}^{n-1} \frac{1}{\eta_{\beta_i}} \frac{(t_i - t_{i-1})^{\beta_i}}{\Gamma(\beta_i + 1)} \sigma_0 + \frac{\sigma_0}{\eta_{\beta_n} \Gamma(\beta_n + 1)} (t - t_{n-1})^{\beta_n} & \sigma_0 \leq \sigma_s \\ \sum_{i=1}^{n-1} \frac{1}{\eta_{\beta_i}} \frac{(t_i - t_{i-1})^{\beta_i}}{\Gamma(\beta_i + 1)} \sigma_0 + \frac{\sigma_0}{\eta_{\beta_n} \Gamma(\beta_n + 1)} (t - t_{n-1})^{\beta_n} + \frac{\sigma_0 - \sigma_s}{\eta_s} t^\gamma E_{1,1+\gamma}(\lambda t) & \sigma > \sigma_s \end{cases} \quad (6)$$

High temperature creep test for mudstone

Experimental set-up and process

The MTS810 electro-hydraulic servo material test system and MTS652.02 high temperature furnace were used for this experiment. The creep test was a step-by-step loading process for each sample; each step involved loading for a certain duration to obtain creep curves of samples under different stress levels. The testing results showed little discreteness for the same sample. After taking the experimental conditions and time into consideration, a multi-stage loading creep test was adopted.

The high temperature creep test for mudstone can be divided into two main processes: Heating of rock samples. The rock samples were wrapped by asbestos and put into high temperature furnace. The temperature was increased to 700 °C at a rate of 5 °C/min and then held at 700 °C for 0.5 hours. Loading for rock samples. Five loading steps were designed for the creep test of mudstone at 700 °C by using uniaxial compression: add pressure to first loading level (3.0 kN) and maintain for 1800 s, add pressure to second level loading (4.5 kN) and maintain for 1800 s, add pressure to third loading level (6.0 kN) and maintain for 1800 s, add pressure to fourth loading level (7.5 kN) and maintain for 1800 s, stop loading until the failure of rock samples is achieved.

Viscoelastic properties for mudstone under high temperature

Creep curves of mudstones under different loads at 700 °C are obtained according to the time history curves of strain, fig. 3(a). A complete creep characteristic curve involves four stages, including the instantaneous elastic deformation (S_E), decay creep (S_1), steady creep (S_2) and accelerated creep (S_3) in fig. 3(b). When the loading is 26.41 MPa, the creep characteristic curve of mudstone contains four stages; when the loading levels were 9.76 MPa, 16.65 MPa, or 19.65 MPa, the curve only contains three stages, fig. 3(a). Therefore, the creep curve with 26.41 MPa is taken as a typical example to investigate the viscoelastic characteristics of mudstone in the creep deformation process under high temperature conditions. Through segmentation treatment and change of strain rate, the whole process can be divided into four stages, including the instantaneous elastic deformation ($0 \leq t \leq t_1$), decay creep ($t_1 \leq t \leq t_2$), steady creep ($t_2 \leq t \leq t_3$), and accelerated creep ($t \geq t_3$) when loading levels was 26.41 MPa.

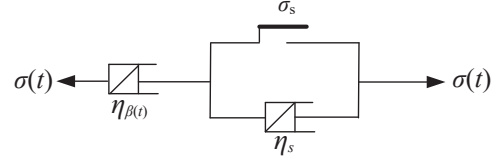


Figure 2. Variable order damaging creep model

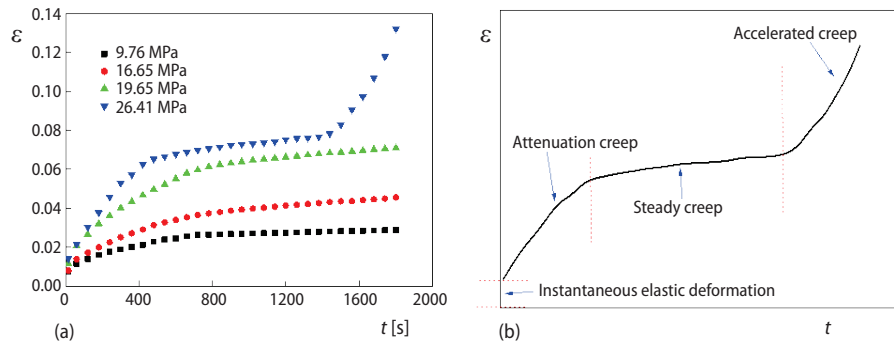


Figure 3. Creep characteristic curve of mudstone at 700 °C; (a) creep characteristic curves with different loading levels, (b) classification of creep deformation stages

(1) The instantaneous elastic deformation stage

In this stage, the deformation of mudstone exhibits complete elastic features, the order $\beta_1 = 0$. Taking it into eq. (9) gives:

$$\eta_{\beta_1} = \frac{\sigma_0}{\varepsilon_v(t_1)}$$

(2) The process of decay and steady creep

In this stage, the creep constitutive relation of mudstone can be obtained as follows:

$$\begin{aligned} \varepsilon(t) &= \sum_{i=1}^{n-1} \frac{1}{\eta_{\beta_i}} \frac{(t_i - t_{i-1})^{\beta_i}}{\Gamma(\beta_i + 1)} \sigma_0 + \frac{\sigma_0}{\eta_{\beta_n} \Gamma(\beta_n + 1)} (t - t_{n-1})^{\beta_n} = \\ &= \varepsilon(t_{n-1}) + \frac{\sigma_0}{\eta_{\beta_n} \Gamma(\beta_n + 1)} (t - t_{n-1})^{\beta_n} \quad n = 1, 2 \end{aligned} \quad (7)$$

Taking the natural logarithm to both sides of eq. (7) gives:

$$\ln[\varepsilon(t) - \varepsilon(t_{n-1})] = \ln \frac{\sigma_0}{\eta_{\beta_n} \Gamma(\beta_n + 1)} + \beta_n \ln(t - t_{n-1}) \quad n = 1, 2 \quad (8)$$

Assume the following relation:

$$\begin{cases} x = \ln(t - t_{n-1}) \\ y = \ln[\gamma_v(t) - \gamma_v(t_{n-1})] \end{cases} \quad (9)$$

The relationship between x and y was fitting by least square method according to the experimental data. Figures 4(a) and 4(b) show the relationships in decay creep and stable creep processes, respectively.

(3) The accelerated creep stage

The creep relation can be expressed as follows:

$$\begin{aligned} \varepsilon(t) &= \sum_{i=1}^3 \frac{1}{\eta_{\beta_i}} \frac{(t_i - t_{i-1})^{\beta_i}}{\Gamma(\beta_i + 1)} \sigma_0 + \frac{\sigma_0}{\eta_{\beta_4} \Gamma(\beta_4 + 1)} (t - t_3)^{\beta_4} + \frac{\sigma_0 - \sigma_s}{\eta_s} t^\gamma E_{1,1+\gamma}(\lambda t) = \\ &= \varepsilon(t_3) + \frac{\sigma_0}{\eta_{\beta_4} \Gamma(\beta_4 + 1)} (t - t_3)^{\beta_4} + \frac{\sigma_0 - \sigma_s}{\eta_s} t^\gamma E_{1,1+\gamma}(\lambda t) \end{aligned} \quad (10)$$

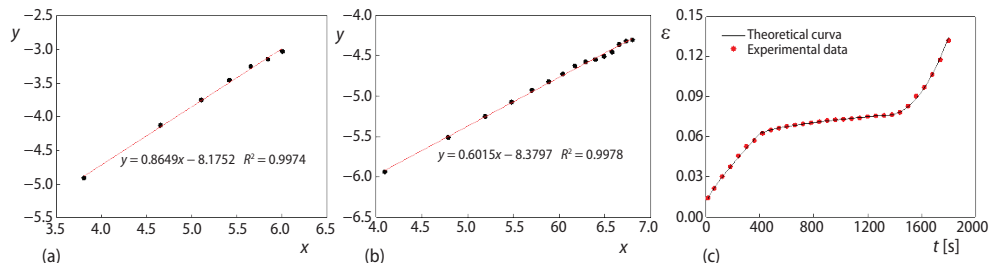


Figure 4. Fitting of creep model parameters with 26.41 MPa; (a) decay creep stage, (b) stable creep stage, (c) theoretical model and experimental data

The order β_i is achieved by the fitting formula, and the viscosity coefficient of mudstone η_{β_i} is obtained after taking β_i into eq. (10). Table 1 shows the orders and viscosity coefficient of mudstone with loading stress of 26.41 MPa at 700 °C. The creep model is then obtained by taking the parameters into eq. (10). Figure 4(c) shows the comparison between the theoretical model and the experimental data. It can be seen that the theoretical model is consistent with the experimental data because the fitting correlation coefficients are greater than 0.99, and the built creep model can effectively reflect each deformation stage of mudstone.

The same method is used to extract the fitting curves of x-y relationships with the other three loading stress levels and corresponding parameters. The models are then compared with the experimental data (tab. 3).

Tables 1, 2, and 3 show the following results: when mudstone is at instantaneous elastic deformation stage, $\beta_1 = 0$; when mudstone comes into the creep deformation stage, both β_2 and β_3 are greater than 0.5 at either the decay creep deformation stage or the stable creep deformation stage, indicating that viscosity is dominant at these two stages according to the relationship between the order and viscoelastic characteristics. However, under the continuous loading stress of 26.41 MPa, the internal damage of mudstone together with the continuous hot melting and thermal evaporation effects at 700 °C lead to the structural damage of mudstone samples, which means that the samples have come into accelerated creep stage. In accelerated creep stage, it is not the viscoelastic stage but viscoplastic stage. Therefore, we cannot analyze the $\beta(t)$ to exhibit the viscoelastic revolution.

What is more, there is a close relationship between the viscoelastic characteristics and the internal composition. Thus, X-Ray Diffraction (XRD) technology was used to analyze the compositions of mudstone materials at room temperature (20 °C) and 700 °C, tab. 4.

Table 1. Parameters of S_E , S_1 , and S_2 under 26.41 MPa

| Parameters | S_E | S_1 | S_2 |
|------------------|----------|---------------------|---------------------|
| β_i | 0 | 0.8649 | 0.6015 |
| η_{β_i} | 687.0758 | $9.8716 \cdot 10^4$ | $1.2878 \cdot 10^5$ |

Table 2. Parameters of S_3 under 26.41 MPa

| Parameters | β_4 | η_{β_4} | η_s | λ | γ |
|------------|-----------|---------------------|---------------------|-----------|----------|
| S_3 | 0.66 | $1.0354 \cdot 10^5$ | $8.1253 \cdot 10^6$ | 12.11 | 0.22 |

Table 3. Parameters with the other three loading stress levels

| Loading stress | Parameters | S_E | S_1 | S_2 |
|----------------|------------------|---------------------|---------------------|---------------------|
| 9.76 MPa | β_i | 0 | 0.5756 | 0.9638 |
| | η_{β_i} | $1.2626 \cdot 10^3$ | $2.5240 \cdot 10^4$ | $3.3962 \cdot 10^6$ |
| 16.65 MPa | β_i | 0 | 0.5891 | 0.8081 |
| | η_{β_i} | $2.0683 \cdot 10^3$ | $3.0673 \cdot 10^4$ | $5.5247 \cdot 10^5$ |
| 19.65 MPa | β_i | 0 | 0.6095 | 0.6535 |
| | η_{β_i} | $1.6824 \cdot 10^3$ | $2.4481 \cdot 10^4$ | $1.8520 \cdot 10^5$ |

Table 4. The main compositions of mudstone

| T [°C] | Maximum diffraction intensity I _{max} (counts) | | | | |
|--------|---|-----------|--------------|------|--------|
| | Quartz | Kaolinite | Cronstedtite | Mica | Illite |
| 25 | 6168 | 963 | 853 | 307 | 0 |
| 700 | 5206 | 0 | 0 | 380 | 491 |

material interconnecting the internal particles of mudstone; and cronstedtite is a kind of iron silicon complex oxide whose particles are quite rigid. The disappearance of these two components greatly decreases the compressive strength of mudstone. Illite is a typical silicate mineral with an aquifer structure, and it possesses a strong thermoplastic deformation capability, which could be used to improve the viscosity of mudstone in the creep process. This is also the main reason why the viscosity property is dominant for the mudstone creep process at 700 °C.

Results regarding β_2 and β_3 are analyzed by comparing the trend of the orders at each creep deformation stage over the stress levels in tab. 3 and 4. β_2 , the order at decay creep stage, increases gradually with the increase of stress level, indicating that viscosity also strengthens during the creep process. This is mainly due to the crack propagation and the occurrence of new cracks within the mudstone after instantaneous elastic deformation. Accordingly, the internal porosity of mudstone increases greatly with increasing load levels. The greater the deformation hysteresis is, the more dominant the viscosity performance is β_3 , the order at the stable creep stage, decreases gradually with increasing stress level, indicating that the viscosity performance fades away gradually, while elastic performance is more dominant. At this stage, the internal damage is mainly from the expansion of the micro cracks and the intersection of cracks. With increasing loading level, porosity decreases gradually as the internal pore closure becomes even more significant. As a consequence, the friction among the internal particles of mudstone increases, and the whole elastic deformation is more significant while the viscosity performance decreases.

Conclusion

The MTS810 electro-hydraulic servo material test system and MTS652.02 high temperature furnace were used to perform the uniaxial creep test for mudstone at 700 °C. A variable-order fractional damaged creep model under high temperature was proposed, and the viscoelastic evolution of mudstone in the creep process were analyzed and studied through the variable-order function in new model. The X-ray diffraction (XRD) technology was applied to distinguish compositions of mudstone for explaining viscoelastic properties and evolution from micro-cosmic aspect.

Acknowledgment

This work was supported by the National Basic Research Program of China (No. 2015CB251601), National Natural Science Foundation (51322401, 51421003), the Fundamental Research Funds for the Central Universities (No. 2014YC09, 2014ZDPY08) (China University of Mining and Technology), the 111 Project (No. B07028).

References

- [1] Li, Y., et al., A Survey on Fractional-Order Iterative Learning Control, *Journal of Optimization Theory and Applications*, 156 (2013), 1, pp. 127-140
- [2] Yang, X. J., et al., On a Fractal LC-Electric Circuit Modeled by Local Fractional Calculus, *Communications in Nonlinear Science and Numerical Simulation*, 47 (2017), June, pp. 200-206

Table 4 exhibits that kaolinite and cronstedtite have disappeared, but Illite has produced. At the same time, the contents for both quartz and mica have hardly changed. It is well known that mudstone is a typical clay rock. Kaolinite is an important bonding

- [3] Yang, X. J., A New Integral Transform Operator for Solving the Heat-diffusion Problem, *Applied Mathematics Letters*, 64 (2017), Feb., pp. 193-197
- [4] Xu, M. Y., Tan, W., Intermediate Processes and Critical Phenomena: Theory, Method and Progress of Fractional Operators and Their Applications to Modern Mechanics, *Science China Physics, Mechanics and Astronomy*, 49 (2006), 3, pp. 257-272
- [5] Mainardi, F., An Historical Perspective on Fractional Calculus in Linear Viscoelasticity, *Fractional Calculus and Applied Analysis*, 15 (2012), 4, pp. 712-717
- [6] Paola, M. D., et al., Fractional Differential Equations and Related Exact Mechanical Models, *Computers and Mathematics with Applications*, 66 (2013), 5, pp. 608-620
- [7] Bagley, R. L., et al., A Theoretical Basis for the Application of Fractional Calculus to Viscoelasticity, *Journal of Rheology*, 27 (1983), 3, pp. 608-620
- [8] Coimbra, C. F. M., Mechanics with Variable-Order Differential Operators, *Annalen der Physik*, 12 (2003), 11-12, pp. 692-703
- [9] Soon, C. M., et al., The Variable Viscoelasticity Oscillator, *Annalen der Physik*, 12 (2005), 6, pp. 378-389
- [10] Ramirez, L. E., Coimbra, C. F., A Variable Order Constitutive Relation for Viscoelasticity, *Annalen der Physik*, 16 (2007), 7-8, pp. 543-552
- [11] Atangana, A., Cloot, A. H., Stability and Convergence of the Space Fractional Variable-order Schrödinger Equation, *Advances in Difference Equations*, 80, (2013), 1, pp. 1-10
- [12] Bazhlekova, E. G., Dimovski, I. H., Exact Solution for the Fractional Cable Equation with Nonlocal Boundary Conditions, *Central European Journal of Physics*, 11 (2013), 10, pp. 1304-1313
- [13] Sun, H. G., et al., A Comparative Study of Constant-Order and Variable-Order Fractional Models in Characterizing Memory Property of Systems, *The European Physical Journal Special Topics* 193, (2011), 1, pp. 185-192
- [14] Razminia, A., et al., Solution Existence for Non-Autonomous Variable-Order Fractional Differential Equations, *Mathematical and Computer Modelling*, 55 (2011), 3, pp. 1106-1117
- [15] Zhang, S., Existence and Uniqueness Result of Solutions to Initial Value Problems of Fractional Differential Equations of Variable-Order, *Journal of Fractional Calculus and Applications*, 4, (2013), 1, pp. 82-98
- [16] Yang, X. J., Machado, J. A. T., A New Fractional Operator of Variable Order: Application in the Description of Anomalous Diffusion, *Physica A: Statistical Mechanics and its Applications*, 481 (2017), Sept., pp. 276-283
- [17] Valerio, D., Da Costa, J. S., Variable-Order Fractional Derivatives and Their Numerical Approximations, *Signal Processing*, 91 (2011), 3, pp. 470-483
- [18] Bhrawy, A. H., Zaky, M. A., Numerical Simulation for Two-Dimensional Variable-Order Fractional Non-linear Cable Equation, *Nonlinear Dynamics*, 80 (2015), 1-2, pp. 101-116
- [19] Yang, X. J., New Rheological Problems Involving General Fractional Derivatives within Nonsingular Power-Law Kernel, *Proceedings of the Romanian Academy - Series A*, 69, (2017), 3, in press
- [20] Yang, X. J., New General Fractional-Order Rheological Models within Kernels of Mittag-Leffler Functions, *Romanian Reports in Physics*, 69, (2017), 4, Article ID 118
- [21] Yang, X. J., et al., New Rheological Models within Local Fractional Derivative, *Romanian Reports in Physics*, 69 (2017), 3, pp. 113
- [22] Yang, X. J., et al., Anomalous Diffusion Models with General Fractional Derivatives within the Kernels of the Extended Mittag-Leffler Type Functions, *Romanian Reports in Physics*, 69, (2017), 4, Article ID 115